Pergamon

Geochimica et Cosmochimica Acta, Vol. 62, No. 21/22, pp. 3407–3412, 1998

0016-7037/98 $19.00 + .00

PII S0016-7037(98)00251-8

Determination of growth rates of (100) and (110) faces of synthetic goethite by scanning force microscopy

P. G. WEIDLER,[1,*] S. J. HUG,[2] T. P. WETCHE,[3] and T. HIEMSTRA[4]

[1]Institut für Terrestrische Ökologie/Bodenchemie, ETH Zürich, CH-8952 Schlieren, Switzerland
[2]Eidgenossisches Anstalt für Wasserversorgung, Abwasserreinigung und Gewässerschutz (EAWAG), CH-8600 Dübendorf, Germany
[3]Department of Plant Biology and Biogeochemistry, Risø National Labortaory and Department of Chemistry, Royal Veterinary and Agricultural University, Copenhagen, Denmark
[4]Department of Soil Science and Plant Nutrition, Wageningen Agricultural University, Wageningen, The Netherlands

(*Received December* 8, 1997; *accepted in revised form July* 24, 1998)

Abstract—For the first time, the growth rate of the (100) and (110) faces of goethite has been measured in situ with scanning force microscopy. Submicron sized goethite particles were immersed in aerated aqueous Fe(II)solutions, whereby Fe(III) was formed by oxidation of Fe(II) by oxygen. Oxidation of Fe(II) is an important and ubiquitous geochemical process in soils and sediments exposed to changing redox conditions. The SFM measurements confirmed that Fe(II) oxidation is catalyzed by goethite and showed that Fe(III) is incorporated on the existing crystal faces. The growth velocity of the (100) face exceeded the one of the (110) faces by about a factor of 1.5 at the experimental conditions of this study (10 mM $FeSO_4$ and KCl, 5mM acetate, pH 5). The different growth rates result in a predominance of (110) faces, which is also observed when goethite is formed in oversaturated Fe(III) solutions at pH 9, and explains the generally observed morphology of goethite particles. The growth behavior appears to be reaction controlled rather than transport controlled. The preferential growth on the (100) faces could be driven by steric factors, in that the grooves on the (100) faces formed by rows of missing oxygens provide preferred sites for Fe incorporation. The surface properties on the different crystal faces are discussed in the frame of CD-MUSIC model. *Copyright © 1998 Elsevier Science Ltd*

1. INTRODUCTION

The primary charging behavior of metal(hydr)oxide surfaces is of great practical and theoretical importance for the understanding of sorption processes on this surfaces. Recent models related the crystallographic data with the charging behavior of these mineral phases (Hiemstra et al., 1996; Hiemstra and van Riemsdijk, 1996). Therefore, knowledge of the abundance of crystal faces of these materials is necessary to predict correct charging curves. For goethite, the ratio of the (110) and (100) faces has some impact on the prediction of the charging behavior of this mineral phase, due to the different number and type of surface groups on these crystal faces.

Furthermore, the growth of Fe(hydr)oxides, such as goethite from ferrous iron solutions plays an important role in redoximorphic soils. In these systems the ferric iron is supplied via the oxidation of ferrous iron. This step should exhibit a major influence on the overall crystallization of these Fe(hydr)oxides. In addition, the valence state, ferrous against ferric, increases drastically the mobility of the iron in such natural systems.

The crystal morphology of goethite has been evaluated by Cornell et al. (1974). Three important types of crystal faces have been reported: the (100), (100), and (001) faces (according to space group #62, Pbnm setting). In contrast, Schwertmann (1984) has shown that (110) faces are the dominating faces on most natural and synthetic goethites, followed by (021) and (100) faces. Furthermore, these crystals were elongated along the crystallographic c-axis with (021) faces as endfaces, which terminate the crystal in this directon. Hence, from crystallographic reasoning, the (021) must be the fastest growing face when compared to the (110) and (100) face, and due to the low abundance of (100), this face must be faster growing than the (110) face (Kleber, 1990). One reason was reported by Weidler et al. (1996), who attributed vicinal faces on the (100) to be responsible for a larger growth rate.

For this study an atomic force or scanning probe microscope (AFM/SPM) (Binnig et al., 1986; Eggleston, 1994) was used to investigate the growth rate of goethite (100) and (110) crystals faces for the first time. This technique has the opportunity of giving direct insight into the topography and mechanical properties of surfaces. It can be used under ambient conditions, e.g., under water or at room temperature. In general, no vacuum or special preparation procedures (e.g., metal coating) are needed.

2. MATERIALS AND METHODS

2.1. Preparation and Characterization of Goethite

The goethite was produced following the procedure in Schwertmann and Cornell (1991). 360 mL of 5 M KOH solution, 200 mL of 1 M $Fe(NO_3)_3$ solution, and 4000 mL H_2O were reacted for 60 h at 70°C. The suspension was stirred 3 times for about 1 min within 24 h. The precipitate was washed with distilled water, dialyzed until free of nitrate, and freeze-dried. The dry product was ground in an agate mortar by hand to obtain a homogeneous goethite preparation.

XRD work was carried out on a SCINTAG XDS 2000 equipped with a Peltier cooled Li drifted Si scintillation counter with Cu-K_α radiation ($\lambda = 0.5418$ nm). The diffractograms were recorded from 17°–107° 2θ with 0.03° 2θ steps and 10 seconds counting time. LaB_6 had been added as an internal standard. Integral line widths of the Bragg peaks were determined by applying the Rietveld structure refinement (Schneider and Dinnebier, 1991; Young, 1993) and single line fitting routines. From these line widths, mean coherence lengths (MCL) were calcu-

*Author to whom correspondence should be addressed (weidler@ito.umnw.ethz.ch).

lated following the approach of Williamson and Hall (1953) and by applying the Scherrer formula (Klug and Alexander, 1974).

Specific surface area was determined with a Micromeritics Gemini 2000 adsorption device using N_2 at 77.3 K. The molecular cross-sectional area was assumed to be 0.162 nm^2. The sample was outgassed at 95°C for 12 h in a stream of nitrogen gas. Measured adsorption data in the partial pressure range from 0.001 to 0.3 p/p_o (p_o saturation pressure) were used for the calculation of the BET surface area and microporosity.

2.2. SFM and Sample Preparation for Scanning

The SFM utilized for this work is a Nanoscope III from Digital Instruments, Santa Barbara, California, USA, equipped with the commercial glass liquid cell. Oxide sharpened Si_3N_4-Cantilevers (Olympus OMCL-RS series) were used. The Fe-containing solution was held in an open syringe, which was connected to the liquid cell by Teflon hosts. Every 30 min the solution in the liquid cell was renewed. Some basic principles of the SFM-technique were reviewed in Binnig et al. (1986), Wickramasinghe (1990), and Eggleston (1994); details of the instrument are described in Anonymous (1993).

Goethite was suspended in a 0.01 M $NaNO_3$ solution and the pH was set to 5.6. Commercially available glass slides, as used in routine light microscopy, were cut into smaller platelets (8 mm diameter) to fit into the liquid cell. These platelets were washed in 6 M HCl for 20 min, afterwards thoroughly rinsed in doubly distilled water for another 20 min, and subsequently transferred into the goethite suspension. After one to several hours, depending on the desired coverage, the glass slides were removed, gently flushed with doubly distilled H_2O, and oven dried at 95°C for 2 h.

2.3. Reaction with Fe(II) Solution

The reaction solution was prepared as follows: 28 mg $FeSO_4 \cdot 7\,H_2O$ were dissolved in 1 mL 2 mM HCl, then mixed with 9 mL solution containing 0.01 M KCl and 5.5 mM pH 5.0 acetate buffer. The final solution was 10 mM in Fe(II), SO_4^{2-}, K^+, and Cl^- and 5 mM in acetate. The pH after mixing was 4.8–4.9. The speciation of Fe(II) in this solution is 65.2% Fe^{2+}, 31.3% $FeSO_4$, and 3.5% $FeAc^+$ and less than 1.22×10^{-7} M $Fe(OH)^+$, as calculated with complex formation constants of 1.22 for FeAc and 1.844 for $FeSO_4$ (values from Smith and Martell, 1979, corrected for I = 0.01 with the Davies equation).

The Fe(II) solution was prepared with rather high Fe(II) concentrations in order to achieve conditions under which Fe(II) was more likely to oxidize at the goethite surface than in solution at a rate leading to observable growth of new solid phase within a few hours. This required that

1) The Fe(II) concentration had to be sufficiently high for adsorption of Fe(II) species on the goethite surface at the rather low pH of 4.9.
2) A pH of 4.9 prevented fast oxidation of Fe(II) in solution, which could have led to precipitation of other Fe(III) phases from the solution. To avoid the precipitation, the rate of Fe(III) formation in solution had to be lower than the rate of incorporation of Fe(III) into the goethite crystal lattice. As we will show, the rate of oxidation of Fe(II) on the goethite surface and formation of new goethite phase exceeded the estimated rate of Fe(II) oxidation in the solution.
3) The presence of Fe(III) in the stock solutions had to be excluded, as this led to immediate precipitation of some Fe(III) in the reaction solution (with subsequent precipitation catalyzed on the surface of suspended small particles). While pH 4.8 solutions prepared with $FeSO_4$ stock solutions remained clear and colorless for at least 30 min after mixing, solution prepared with $FeCl_3$ turned brown and turbid within minutes.

3. RESULTS AND DISCUSSION

XRD and Rietveld structure refinement revealed that the product was pure goethite. The mean coherence length, which is a measure for the mean crystallite size, was 9.0 ± 0.1 nm following the approach of Williamson and Hall (1953). The single line fitting routine considered possible anisotropic line broadenening, and this procedure resulted in MCL values of 6 nm in the [100] direction, 14 nm in [010], and 11 nm in [001]. The specific surface area was 38.1 m^2/g, to which micropores contributed 6.1 m^2/g or 16.0%. The pH of the reactive Fe(II) solution remained constant at 4.85 during 4 hours of the SFM measurements, and slightly brownish tinge was observed in the clear solution.

Images were obtained in various time steps within 3 hours and 55 minutes. After one to two images (scan rate 1 Hz), the set point had to be readjusted to the minimum value of approximately 5 nN. Otherwise no useful images could have been obtained, as found in prelimenary experiments carried out under the same conditions. Four representative images are shown in Fig. 1. We choose the deflection mode for presentation purposes, due to the more 3D-like appearance of the crystals in this mode, but the instrumental settings (e.g., gains) were optimized for the height mode imaging. The width of the (100) face decreased with time. In addition, three flat islands appeared on the (100) face after approximately 1 hour and remained to the end of the experiment (Fig. 1d). Unfortunately, no reliable data were obtained during the experiment for the changes of the length in the direction of the c-axis of the crystal, because the other end of the crystal was covered by another larger crystal, which also increased in its size.

Cross sections at five different locations perpendicular to the crystallographic c-axis were chosen, and the lengths in vertical and horizontal direction and angles between the different line segments were measured. Thus the identification of the precipitated material and crystal faces could well be established. The mean value of the angle formed by (100) and (110) faces calculated from 100 measurements was 157.3° ± 0.8°, which corresponds to a mean deviation from the theoretical value (155.2°) of 1.4%. This value is different from the angle found for the (110) and $(1\bar{1}0)$ faces, which is 130.4°. Hence, the three major crystal faces depicted in Fig. 1 are the (100) face (grey area), and adjacent to both sides of this face, the (110) faces (light grey and black/dark grey areas).

Figure 2 shows the change of height of the crystal faces. The cross sections were perpendicular to the c-axis of the crystal. The heights in the [100] direction and in the [110] direction were calculated from the measured width of the (100) face and the measured angle between the (100) and (110) plane. The growth in the [100] direction was faster than in the [110] direction. This behavior is demonstrated in Fig. 3. Furthermore, a decrease in the growth rate was observed after 120 minutes. The slopes obtained by fitting a linear regression to the change of heights of the respective sections per time are stated in Table 1. The calculated 95% confidence intervals for the mean rates of each crystal face obtained from the linear regressions of the data of each cross section were not overlapping. The ratio between the mean growth rates of the (100) and (110) face was 1.5 for the fast rates, and 2.5 for the slow rates. The increase in this ratio coincided with the decrease of the growth rate to approximately 28% of the initial one. The (100) growth rate decreased to 11% of its initial rate.

The (100) face of the goethite had no vicinal faces, and remained flat throughout the experiment, despite the three flat islands on the (100) face, which exhibited an average height corresponding to one to two unit cells (Fig. 1b–d). Their area

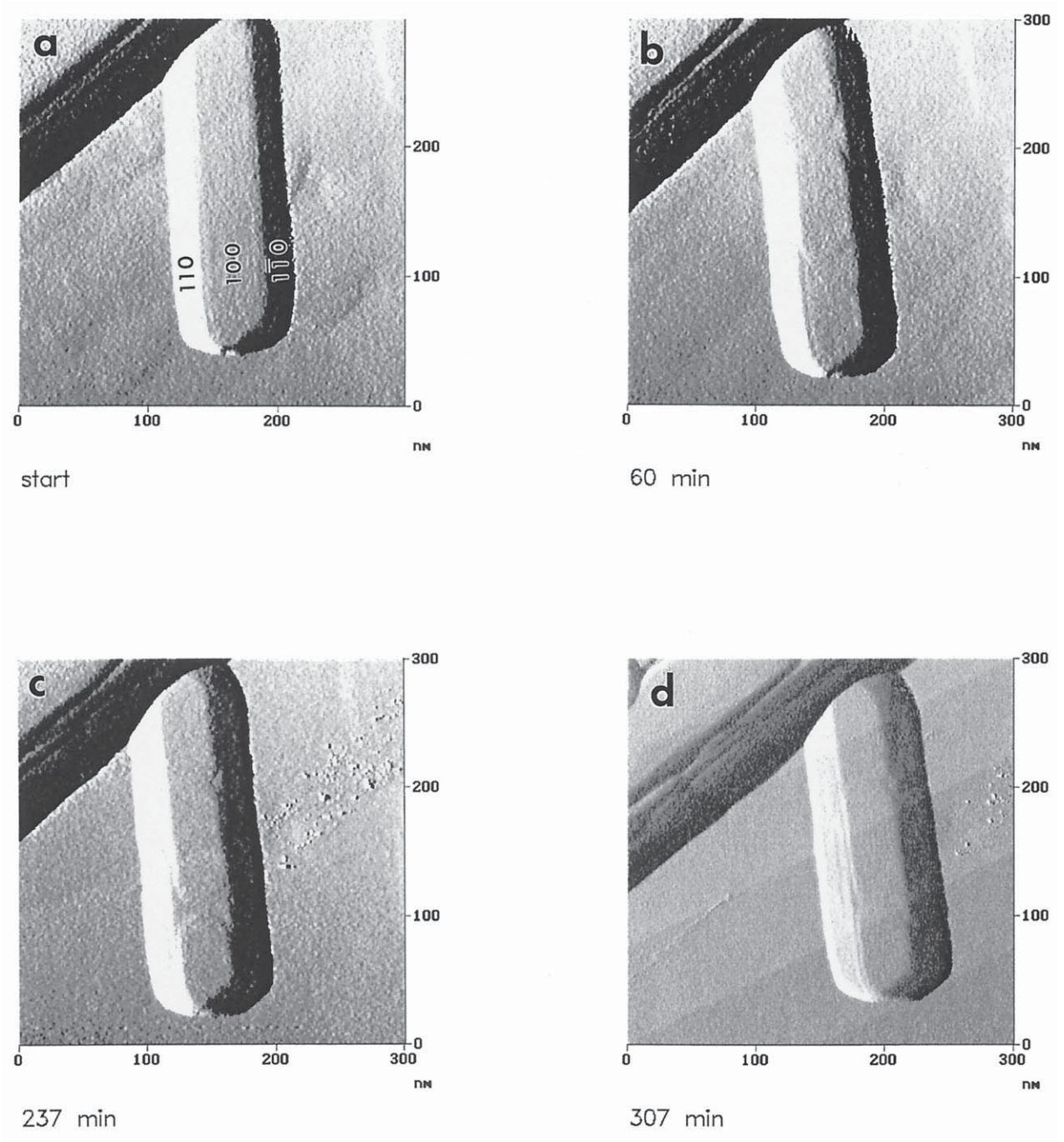

Fig. 1. Deflection mode images of the goethite used in the growth experiment. The images were taken at the (a) beginning, (b) after 60 minutes, (c) after 237 minutes, and (d) after 307 minutes. After 61 minutes patches developed, which spread only over the (100) face. Images (a–c) are enlargements of 650 nm scans.

was approximately 30×50 nm^2 and was, therefore, about 10 times larger than the size of the coherent scattering domains (approximately. 10×16 nm^2, as determined by XRD). As reported by Weidler et al. (1996) and confirmed in this study, no screw dislocation were detected. Therefore, other explanations than growth by vicinal faces or surface defects has to be found for the observed growth behavior.

One possibility is that the difference in rates between different crystal faces is directly related to the different charge density of these crystal faces at the pH of our experiments (4.8–4.9). The surface charge of specific crystal faces can be calculated from the CD-MUSIC model (Hiemstra and van Riemsdijk, 1996) in which an electrostatic model involving the specific surface structure (assuming no relaxation or reconstruction) and a surface complexation model are combined. The site density of the reactive groups is derived from the crystal

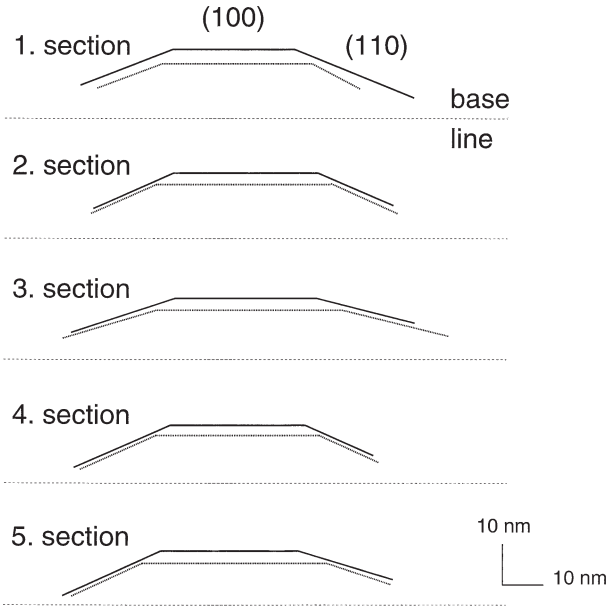

Fig. 2. Cross sections taken at different locations and at the beginning (fine dotted line) and after 3 hours 55 minutes (solid line). The horizontal, dotted line is the baseline (surface of glass slide). The crystal faces are indicated.

structure of the mineral phase under consideration, i.e., goethite. The O, OH, or OH_2 surface groups may be coordinated to one, two, or three Fe atoms in the goethite crystal. Depending on the number of these Fe atoms (n), the surface groups are denoted singly ($n = 1$), doubly ($n = 2$), or triply ($n = 3$) coordinated surface groups. The doubly coordinated surface groups are considered to be inert in the normal pH range (Hiemstra et al., 1989), and it has been reasoned that only one third of the triply coordinated surface groups is reactive for protons (Hiemstra and van Riemsdijk, 1996). Due to different approaches to accounting for hydrogen bond formation, two scenarios for the formation of surface charge by protonation of surface sites at $pH < pH_{pzc}$ have been proposed (Venema et al., 1998). One of these results in approximately similar surface charge for (021), (110), and (100) faces at pH 4.8–4.9, and the other leads to a higher positive surface charge for the (021) face as compared to the (110) and (100) faces. For the latter face the surface charge density is assumed to be smaller than the one of the (110) face.

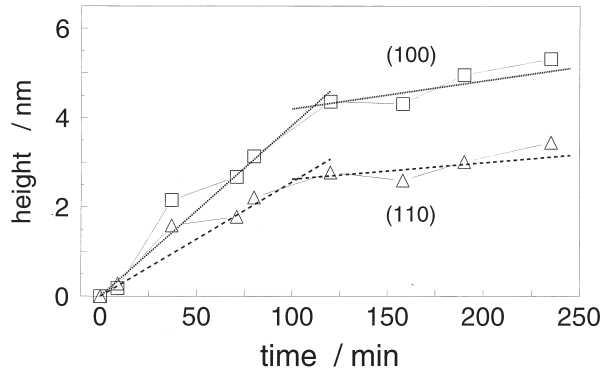

Fig. 3. The averaged increase of height for the (100) (□), and the (110) face (△). The dotted lines indicate the fitted linear regression.

Table 1. Mean growth rates of the (100) and (110) crystal faces of goethite and the width of (100) obtained from linear regression fits to 5 different cross sections. CI = 95% confidence interval; r = correlation parameter; N = number of data points used in the fitting procedure

X-tal face	Section	Rate/nm min^{-1}	CI/nm min^{-1}	r	N
(100)	fast	0.0383	0.0055	0.9922***	6
	slow	0.0148	0.0188	0.9223	4
(110)	fast	0.0256	0.0051	0.9854***	6
	slow	0.0060	0.0113	0.8505	4
Width	section	rate	CI	r	N
(100)	Fast	−0.065	0.018	−0.9815***	6
	slow	−0.007	0.021	−0.7096	4

Significance levels of the correlations are indicated by *<1%, **<0.1%, and ***<0.01%

The dominating Fe(II) species in the present solution is the positive charged $Fe^{2+}(H_20)_6$. From the elongated goethite crystals of this study, which are bounded by (021) faces in the [001] direction, and the ascertained higher growth velocity of the (100) over the (110) faces, and the aforementioned charging behavior of these crystal faces, it can be concluded that electrostatic forces can not be the major driving force for both the transport of the Fe-species from the bulk solution to the crystal surface and the crystallization of these goethite crystals. For otherwise, the (021) face should exhibit the same or the lowest growth velocity in comparison to the remaining two crystal faces.

This finding suggests that either surface structure influences growth by preferred oxidation of Fe(II) on the surfaces or that Fe(III) species are formed in solution which act as building blocks for the growth of the respective crystal faces. What then is the stability of the Fe species in solution? To answer this questions we can estimate the formation rate of Fe(III) from, respectively, the oxidation of Fe^{2+}, $FeOH^+$, and $Fe(OH)_2$ following Stumm and Morgan (1996):

$$d[Fe(III)]/dt = (k_O \times [Fe^{2+}] + k_1 \times [FeOH^+] + k_2 \times [Fe(OH)_2]) \times [O_2] = (10^{-5.1} \times 6.52 \times 10^{-3} + 10^{1.4} \times 1.21 \times 10^{-7} + 10^{6.9} \times 6.99 \times 10^{-14}) \times 0.25 \times 10^{-3} = 9.15 \times 10^{-10} Ms^{-1} \quad (1)$$

The rate constant for the oxidation of $Fe(II)Ac^+$ has not been reported, but can be estimated from the linear free energy relationship (LFER) between log k(oxidation) for Fe^{2+} and their corresponding reduction potentials (Wehrli, 1990). Using this LFER and a reduction potential for $Fe(III)Ac^{2+}/Fe(II)Ac^+$ of 0.64 V (calculated from the corresponding complex formation constants) one obtains an estimated rate constant for oxidation, log $k_{Ac,ox} = -3.12$. This gives an oxidation rate for $Fe(II)Ac^+$:

$$d[Fe(III)]/dt = logk_{Ac,ox} \times [Fe(II)Ac^{+}] \times [O_2]$$
$$= 10^{-3.12} \times 3.46 \times 10^{-4} \times 0.25 \times 10^{-3}$$
$$= 6.56 \times 10^{-11} Ms^{-1}, \quad (2)$$

which adds about 10% to the rate estimated in Eqn. 1. In addition, it has been shown in several studies that millimolar to molar concentrations of sulfate decreases the rate of Fe(II) oxidation (Tamura et al., 1976a; Sung and Morgan, 1980).

Considering that 31% of Fe(II) are present in the form of slower reacting $Fe(SO)_4$, a total rate of Fe(III) formation in solution of 1×10^{-9} M s^{-1} provides an upper estimate. The oxidation rate constant for adsorbed Fe(II) on goethite surfaces has been reported (Tamura et al., 1976b) as log k(FeO_2-Fe^{+}) = 0.7. To compare oxidation rates in solution and at the surface, all rates are given in M s^{-1}, calculated with the SFM liquid cell volume of 40 μL. The accessible area of the glass platelets in the liquid cell had an diameter of 7.25 mm, and was covered to 98% by goethite estimated from several images taken at scan sizes of 150, 50, and 25 μm. The surface area of goethite in the liquid cell is $0.98 \times (7.25/2)^2 \times \pi \times$ mm^2 = 40.5 mm^2 = 4.0×10^{13} nm^2. Assuming 10 sites per nm^2 gives 6.7×10^{-10} moles of sites and a concentration of 1.7×10^{-5} moles L^{-1} surface sites. With all of these occupied, we arrive at an estimated Fe(III) formation rate of $1.7 \times 10^{-5} \times 10^{0.7} \times 0.25 \times 10^{-3} = 2.1 \times 10^{-8}$ M s^{-1}. This rate is larger than the rate of Fe(III) formation in solution, and therefore, the dominating process.

Because Fe(II) oxidation consumes O_2 in the SFM fluid cell, we estimated the time needed to consume 250 μM O_2 with the observed rate of 2.1×10^{-8} M s^{-1}. The obtained value of 13 h exceeded the 30 min period of solution renewal in the liquid cell. Hence, with the previous assumptions made, O_2 depletion due to the Fe(II) oxidation can be ruled out. The decrease of the growth rate after 2 h can be explained by the slow accumulation of precipitates in solution and possibly on the glass walls of the liquid cell. The large surface area formed in this process can also catalyze Fe(II) oxidation and could lead to a depletion of Fe(II).

The observed Fe(III) formation rate was calculated from the growth rate measured by the SFM. For the (100) face one derives 3.1×10^{-8} M s^{-1} for the fast reaction and for the slow one 1.2×10^{-8} M s^{-1}. For the (110) face a value of 2.1×10^{-8} M s^{-1} and 0.5×10^{-8} M s^{-1} is obtained for the fast and slow reaction, respectively (calculated from the observed rate in nm min^{-1}, transformed to mm^3 s^{-1} by multiplying with coverage $\times$ area; subsequent multiplication with the density of goethite, 4.26 g cm^{-3}, a conversion factor of 10^3 ($mm^3 \times cm^{-3}$), and division with the molar weight of goethite, 88.85 g M^{-1}, thus for (100) : $0.0383 \times 40.5 \times 4.26$ / ($60 \times 88.85 \times 10^6 \times 40 \times 10^{-6} \times 10^3$) = 3.1×10^{-8} M s^{-1}. Thus, the observed Fe(II) oxidation rate observed by SFM was 1–2 orders of magnitude (31 times for (100) and 21 times for (110)) larger than the calculated rate of oxidation of Fe(II) in solution and of the same magnitude as the expected rate of oxidation on the surface. Therefore, precipitation in solution is probably of minor importance for the initial growth of goethite under our experimental conditions, and growth is most likely controlled by surface processes.

These surface controlled processes can be divided into (1) the transport of the building units across the crystal surface and (2) the incorporation of the units into the crystal surface sites and formation of new crystalline phase. Both steps can be influenced by the steric environment and specific coordination of the surface oxygens on the particular crystal face. As an example, only singly and doubly coordinated oxygens are found on the (021) face. Without discussing the (021) surface structure in detail, the surface oxygens form groups of 3 or 4 oxygens that are available to become the apices of new Fe-containing octahedra as Fe attaches to these sites during growth. These "open octahedra" are thus sites of preferential iron adsorption and attachment. This is supported by the results of Spadini et al. (1994) and Hiemstra et al. (1996), who found a stronger adsorption of Cd on the (021) face compared to (110).

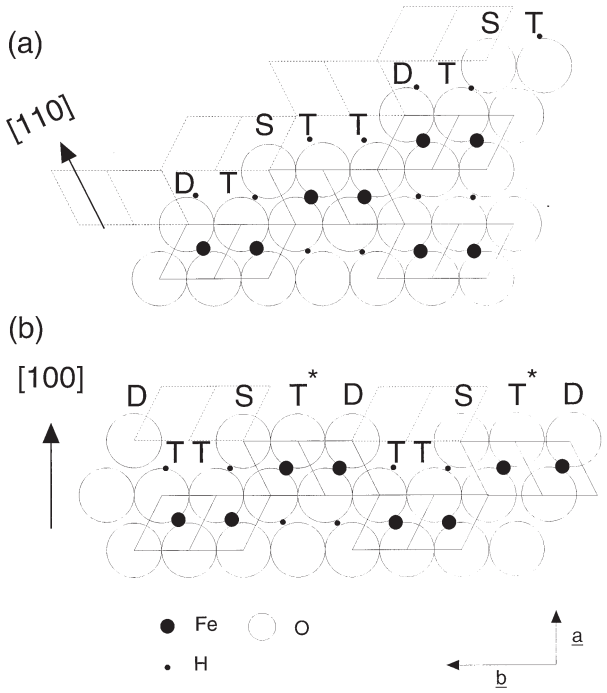

Fig. 4. A sketch of a cross-section of (a) the (110) and (b) the (100) crystal face of goethite viewed parallel to the c-axis. The octahedra indicated by full lines are within the goethite crystal, whereas the ones drawn with dotted lines belong to a new grown goethite layer. S, D, and T indicate singly, doubly, and triply coordinated oxygens, respectively.

An unfavorable situation for Fe attachment is encountered on the (110) face (Fig. 4a). Here, only "closed" octahedra already containing Fe are present, and only proton positions are available on the outermost oxygen layers. The (110) plane is the one with the highest Fe surface density, and its slow growth makes it a highly likely endface for goethite. The situation is different for the (100) face. Missing oxygens form grooves running parallel to the crystallographic c-axis (Fig. 4b). These grooves provide sites for preferred $H_2PO_4^{-}$ sorption as reported by Parfitt et al. (1975), indicating a preference for incorporation of oxygens. The adsorption and subsequent oxidation of an $Fe^{2+}(H_20)_6$ on an S site (see Fig. 4b) on (100) covers the groove. The oxygen site within the groove will be occupied, thus completing a new octahedron. The same process, occurring at adjacent parallel grooves, will lead to formation of a

new set of grooves (Fig. 4b). Hence, the sites of attachment are maintained during growth.

As mentioned above, charging effects on the growth rate cannot be totally excluded. If the positive surface charge of (100) is smaller than on (110) the transport of the Fe^{2+} species to the (100) surface should be faster, resulting in a faster growth rate for the (100), as observed. An Fe^{2+} species approaching a (110) surface would have to encounter a potential barrier that is at least 5 mV higher than on a (100) face (estimated by $\Delta\psi = \ln(1.5) \times RT/(2F)$; with potential ψ R =8 .31 J mol^{-1} K^{-1}, T = 298 K, F = 96491 C mol^{-1}). Even if we double this value to 10 mV, this would correspond to a difference in pH of the point of zero charge of 0.2 between the (110) and (100) surfaces. This small difference is within the accuracy of the CD-MUSIC model (Hiemstra and van Riemsdijk, 1996). In addition, the two surfaces could have a slightly different catalytic effect upon Fe(II) oxidation, and this difference would also likely scale with potential difference between the two surfaces. We cannot rule out an electrostatic effect that influences the relative growth rates of the (110) and (100) surfaces. There are also, as we have discussed above, steric factors related to the specific atomic structure of these surfaces that could account for the differences in growth rate. A definitive answer will have to await further study.

In ongoing studies, the combination of this technique with, e.g., attenuated total reflection Fourier transform IR (ATR-FTIR) allows the study of surface layers with well-defined, custom tailored thickness and compositions. Studies with mixed Cr-Fe solution systems will allow us to track the development of IR bands with increasing layer thickness under solution conditions identical for both SPM and ATR-FTIR.

4. CONCLUSION

Our SFM measurements confirm that Fe(II) oxidation is catalyzed on the goethite surface. Compared to batch experiments, where only the rate of Fe(III) formation in solution can be measured, the SFM measurement provides detailed information that helps constrain conclusions concerning (1) the growth of Fe(III) solid phase, (2) the catalytic activity on different crystal faces, and (3) the structural factors that determine the different rates of Fe(II) oxidation.

As a first example, this in situ observation of the development of the goethite (100) and (110) face showed that the growth velocity of the (100) face exceeds the one for the (110) faces by about a factor of 1.5. We suggest that mainly the oxidation of the ferrous Fe and the incorporation as Fe(III) at the goethite surface drives the crystallization, specifically that the structure of the surface and the steric situation controls the incorporation of Fe. In detail, it is the grooves on the (100) surface, which are formed by missing rows of oxygens, and the neighboring singly and doubly coordinated surface groups, which govern the growth behavior in the [100] direction.

Acknowledgements—The authors gratefully acknowledge the critical reading of this manuscript and helpful discussions by Prof. Dr. W. Stumm (EAWAG, Dübendorf, Switzerland), Prof. Dr. H. C. B. Hansen (KVL, Frederiksberg/Copenhagen, Denmark), and especially Prof. Dr. C. Eggleston (University of Wyoming, Laramie, USA). One of the authors (TPW) acknowledges the support by the Danish Natural Science Research Council.

REFERENCES

Anonymous (1993) Digital Instruments, Nanoscope III Command Reference Manual Version 3.0. Digital Instruments Inc., Santa Barbara, CA, 93103, USA.

Binnig G., Quate C. F., and Gerber. Ch. (1986) Atomic Force Microscope. *Phys. Rev. Lett.* **26(9),** 930–933.

Cornell R. M., Posner A. M., and Quirk J. P. (1974) Crystal morphology and the dissolution of goethites. *J. Inorg. Nucl. Chem.* **36,** 1937–1946.

Eggleston C. (1994) High Resolution Scanning Probe Microscopy: Tip-Surface Interaction, Artifacts and Applications in Mineraolgy and Geochemistry. In *CMS Workshop Lectures, Vol. 7, Scanning Probe Microscopy of Clay Minerals* (ed. K. L. Nagy and A. E. Blum), pp. 1–90. The Clay Minerals Society.

Hiemstra T. and van Riemsdijk W. H. (1996) A surface structural approach to ion adsorption: The charge distribution (CD) Model. *J. Colloid Interface Sci.* **179,** 488–508.

Hiemstra T., van Riemsdijk W. H., and Bolt H. G. (1989) Multisite Proton Adsorption Modeling at the Solid/Solution Interface of (Hydr)oxides: A New Approach I. Model Description and Evaluation of Intrinsic Reaction Constants. *J. Colloid Interface Sci.* **133,** 91–104.

Hiemstra T., Venema P., and van Riemsdijk W. H. (1996) Intrinsic proton affinity of reactive surface groups of metal (hydr)oxides: The bond valence principle. *J. Colloid Interface Sci.* **184,** 680–692.

Kleber W. (1990) Einführung in die Kristallographie. Verlag Technik.

Klug H. P. and Alexander L. E. (1974) *X-Ray Diffraction Procedures.* Wiley.

Parfitt R. C., Russell J. D., and Farmer V. C. (1975) Confirmation of the surface structure of goethite (α-FeOOH) and phosphated goethite by infrared spectroscopy. *J. Chem. Soc. Faraday* 1, **72,** 1082–1087.

Schneider J. and Dinnebier R. E. (1991) Gufi-Wyriet: An integrated PC powder pattern analysis package. *Materials Science Forum* **79-82,** 277–282.

Schwertmann U. (1984) The influence of aluminum on iron oxides: IX. Dissolution of Al-goethites in 6 M HCl. *Clay Mineral.* **19,** 9–19.

Schwertmann U. and Cornell R. M. (1991) *Iron Oxides in the Laboratory.* VCH Weinheim.

Smith R. M. and Martell A. E. (1979) *Critical Stability Constants.* Plenum Press.

Spadini L., Manceau A., Schindler P. W., and Charlet L. (1994) Structure and stability of Cd^{2+} surface complexes on ferric oxides. 1. Results from EXAFS spectroscopy. *J. Colloid Interface Sci.* **168(1),** 73–86.

Stumm W. and Morgan J. J. (1996) Aquatic Chemistry. Wiley.

Sung W. and Morgan J. J. (1980) Kinetics and products of ferrous iron oxygenation in aqueous systems. *Environ. Sci. Technol.* **14,** 561–568.

Tamura H., Goto K., and Nagayama M. (1976a) Effect of anions on the oxygenation of ferrous ion in neutral solutions. *J. Inorg. Nucl. Chem.* **38,** 113–117.

Tamura H., Goto K., and Nagayama M. (1976b) The effect of ferric hydroxide on the oxygenation of ferrous ions in neutral solutions. *Corrosion Sci.* **26,** 197–207.

Venema P., Hiemstra T., Weidler P. G., and van Riemsdijk W. H. (1998) Intrinsic proton affinity of reactive surface groups of metal (hydr)oxides: Application to iron (hydr)oxides. *J. Colloid Interface Sci.* **198,** 282–295.

Wehrli B. (1990) Redox reactions of metal ions at minerals surfaces. In *Aquatic Chemical Kinetics* (ed. W. Stumm), pp. 311–336. Wiley.

Weidler P. G., Schwin, T., and Gau, H. E. (1996) Vicinal faces on synthetic goethite observed by atomic force microscopy. *Clays Clay Mineral.* **44(4),** 437–442.

Wickramasinghe H. K. (1990) Scanning probe microscopy–Current status and future trends. *J. Vac. Sci. Technol.* **A8,** 363–386.

Williamson G.. and Hal, W. H. (1953) X-ray line broadening from filed aluminium and wolfram. *Acta Metall.* **1,** 22–31.

Young R. A. (1993) *The Rietveld Method.* International Union of Crystallography, New York.